LARGE-SCALE SECONDARY FLOWS IN A TURBULENT BOUNDARY LAYER CAUSED BY HIGHLY ORDERED AND DIRECTIONAL SURFACE ROUGHNESS.

***N. Hutchins*[1], *B. Nugroho*[1] *and J. P. Monty*[1]**

[1] ***Walter Bassett Aerodynamics Laboratory***
Department of Mechanical Engineering, University of Melbourne
Victoria 3010 Australia.

nhu@unimelb.edu.au

Abstract

This paper describes initial experimental results from an ongoing investigation into the perturbation of a zero pressure gradient turbulent boundary layer due to a very unusual surface roughness. A highly ordered and directional roughness pattern imposes a large-scale secondary flow onto the boundary layer. This causes a spanwise variation of the boundary layer thickness by a factor of up to 2 (for the strongest cases), in spite of the fact that the peak-to-trough roughness height is only $1/100^{\text{th}}$ of the boundary layer thickness. Initial results suggest that this unique surface roughness is acting as a vortex generator, producing large-scale arrays of counter-rotating streamwise vortices. These rough surfaces do not appear to obey Townsend's outer layer similarity approximation.

1 Highly ordered roughness surfaces

The roughness surface consists of converging-diverging arrangements of riblet-type striations (arranged in a 'herring-bone' pattern). The motivation for this study comes from the investigation by Koeltzsch *et al.* (2002), which indicated that such surfaces could cause large-scale azimuthal variations within fully turbulent pipe-flow. The schematic in Figure 1 defines the key dimensions for the surface. Table 1, lists the key parameters for the 6 experiments detailed in this paper. The cross-section of the riblets is trapezoidal, with an h/s ratio of 0.74. The riblets do not quite represent the classic triangular profile (see for example Bechert *et al.*, 1997) since there is a slight flat in the riblet trough (due to the chamfered tip of the 60° cutter). A detailed view of the riblet cross-section is also given in figure 1. The riblet spacing $s = 0.673$ mm and height $h = 0.5$ mm is fixed for all surfaces. The riblets are yawed at an angle α to the mean flow direction to generate regions of convergence and divergence. Two different yaw angles are investigated, $\alpha = 10^\circ$ and $\alpha = 30^\circ$. For all cases tested, the width of each converging and diverging region is 73.75 mm (such that the repeating spanwise wavelength $\Lambda = 147.5$ mm).

experiment identifier	U_∞ (ms^{-1})	α ($^\circ$)	F_x (m)	s^+	h^+	x (m)
E1	15	30	2.9	23	18	2.9
E2	15	30	1	23	18	2.9
E3	15	10	4	23	18	4
E4	20	10	4	33	25	4
E5	10	10	4	17	13	4
E6	5	10	4	9	6	4

Table 1: Riblet dimensions and flow parameters for the 6experimental configurations. Viscous scaled dimensions (h^+ and s^+ are calculated based on the smooth wall friction velocity U_{τ_s} at the equivalent freestream conditions and x location).

Note that for clarity riblets are not drawn to scale in figure 1 (only 10 riblets are represented per half wavelength $\Lambda/2$, in reality there are approximately 110). By varying the freestream velocity, the viscous-scaled riblet height can be varied (experiments E3 - E6). The other key dimension is F_x, defined as the streamwise fetch. For the 10° converging/diverging angle riblets, a fetch of $F_m = 4$ m is used. The effect of different fetch is explored for the $\alpha = 30^\circ$ riblets with $F_x = 2.9$ m for experiment E1 and $F_x = 1$ m for experiment E2.

To manufacture these surfaces, a three-axis CNC machine was used to create a master tile of the diverging-converging riblet pattern in acetal copolymer. The master tile has dimensions 515×295 mm containing two strips at $+\alpha^\circ$ and two strips at $-\alpha^\circ$ (the master tile dimension assures perfect tessellation in x and y). A mold of this tile was produced in silicone rubber and used to cast multiple polyurethane reproductions of the original tile. The resulting casts were then affixed to the floor of the boundary layer wind tunnel using embedded magnets.

2 Experiments

The experiments were performed in an open-return blower wind tunnel located in the Walter Basset Laboratory at The University of Melbourne. The wind tunnel has a 6.7 m long working section with cross-

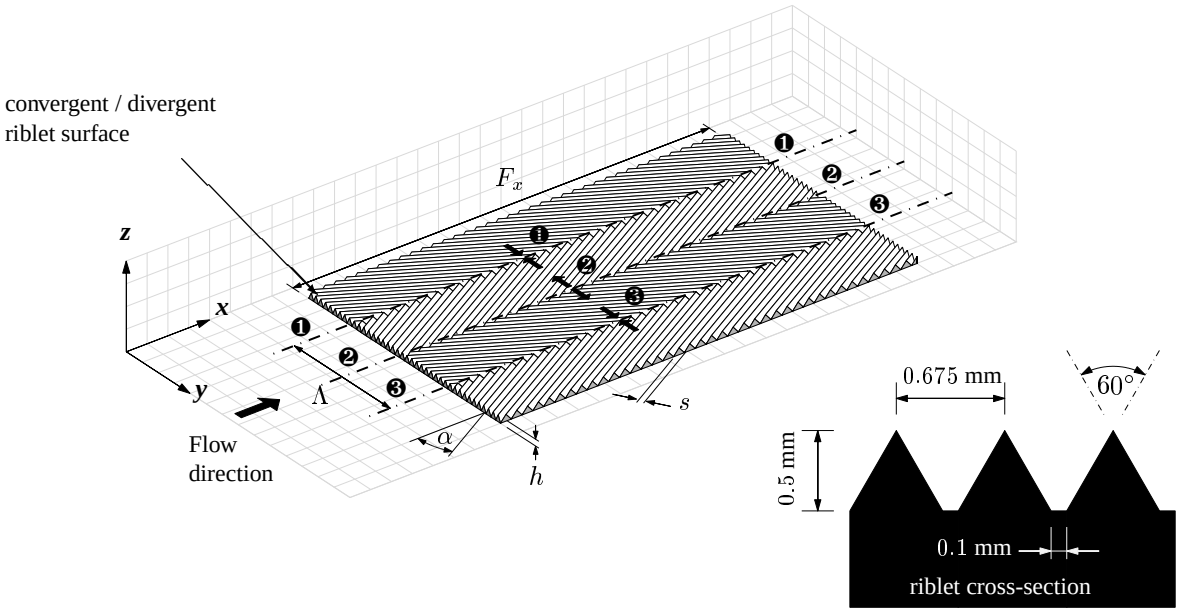

Figure 1: Schematic diagram of converging / diverging riblet pattern, showing expected regions of converging (regions ① and ③) and diverging (region ②) spanwise flow.

sectional area 0.94 x 0.375 m. The roof of the wind tunnel is fully adjustable to enable accurate adjustment of the pressure gradient. All data presented are measured with a single-normal hot-wire probe operated in constant temperature mode using an *AA Lab System AN-1003* anemometer (with overheat ratio set to 1.8). Wollaston wires are soldered to a boundary layer type probe-body geometry (*Dantec 55P15*) and etched to give a 5μm platinum filament of length approximately 1 mm. The length-to-diameter ratio of the etched hot-wire sensors were set to exceed 200 to minimize attenuation due to end conduction. Ligrani & Bradshaw (1987) and Hutchins *et al.* (2009) indicate that the current sensors (which have viscous-scaled length $l^+ \approx 35$), will suffer some attenuation due to insufficient spatial resolution. However, since at this stage these measurements are made for comparative purposes only (between the smooth wall and riblet modified flows), such attenuation is deemed acceptable. Measurements are made at various stations downstream of the tripped inlet to the working section. An automated two-axis traverse (capable of moving in both the spanwise and wall-normal directions) was used to obtain hot-wire measurements over a spanwise / wall-normal plane. A series of 17 boundary layer profiles map the flow characteristics on a plane spanning $-\Lambda/2 < y < \Lambda/2$ in the spanwise direction. Each profile comprises 30 measurements, logarithmically spaced in the wall-normal direction. These measurements reveal the large-scale secondary flows induced by the converging/diverging roughness surface.

3 Results

Experiment E1

Figure 2(a) shows the variation in the mean velocity across the spanwise wavelength of the surface for experiment E1. The wall-normal ordinate is normalised by the boundary layer thickness of the corresponding smooth surface δ_s (at the same streamwise location and freestream velocity). The dot-dashed line in Figures 2 and 3 shows the edge of the boundary layer with the convergent divergent surface installed. The dashed line shows the comparable boundary layer thickness for the smooth surface[1] . It is obvious that the roughness pattern has imposed a large spanwise variation on the mean velocity contours. The boundary layer thickness has a very pronounced variation across the spanwise wavelength, with the thickness varying from $1.9\delta_s$ at the converging regions, to approx $0.9\delta_s$ at the diverging pattern regions. It is remarkable that a surface modification with such a small roughness height ($h/\delta_c \approx 0.01$) can cause such a large spanwise variation in boundary layer thickness. Figure 2(b) shows the fractional change in mean velocity about the corresponding smooth wall case $(U-U_s)/U_s$. The diverging surface regions have lowered the velocity right across the layer (and hence thickened the boundary layer), while the diverging portions lead to increased velocity (and a reduced δ).

To better illustrate the spanwise variation, Figures 3(a & b) show the spanwise variation of the mean and the local standard deviation about the spanwise averaged rough wall result (whereas figure $2b$ previously showed spanwise variation about the smooth wall case). Figure 3(a) shows the spanwise variation in the local mean velocity normalised by the rough wall spanwise average U_{sa} (the subscript *sa* refers to 'spanwise average'). It is again clear that the diverging portion of the riblets ($y/\Lambda = 0$) is characterized by high speed regions, and the converging part ($y/\Lambda = \pm 0.5$)

[1] all boundary layer thicknesses are calculated for the point where the velocity recovers to 98% of the freestream U_∞

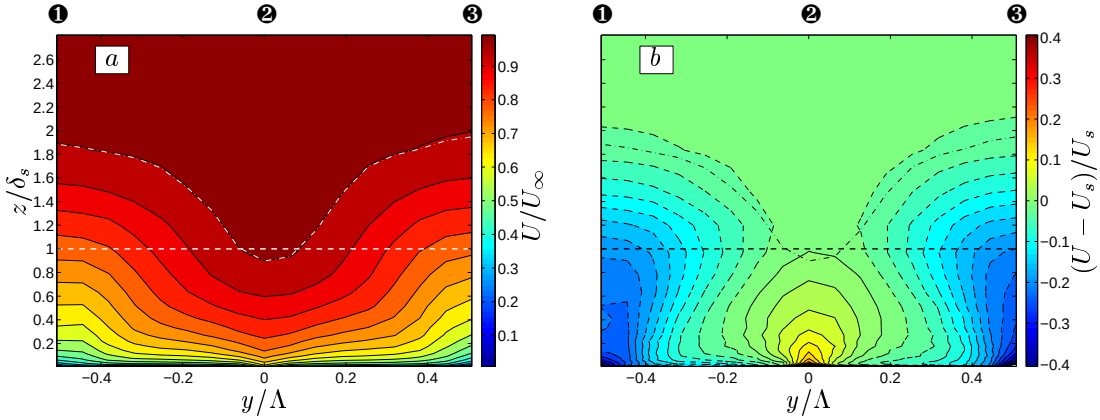

Figure 2: Contours of mean velocity for E1 over a spanwise/wall-normal plane spanning Λ in y direction. Regions of convergence (❶ & ❸) and divergence (❷) are marked on figures. (a) mean velocity normalised by the freestream; (b) mean velocity as a percentage variation about the smooth wall case. Solid and dashed contours show positive and negative values respectively. Dot-dashed line shows δ for rough surface. Dashed line shows smooth wall boundary layer thickness δ_s.

is characterized by low speed regions. Figure 3(b) shows the local standard deviation of streamwise velocity fluctuations u', normalized by the spanwise average value (u'_{sa}). The majority of the boundary layer above the diverging region of the riblets is characterised by reduced turbulence intensity, while the converging regions exhibit predominantly increased intensities. It should be noted that there are regions very close to the wall, where this behaviour seems to be reversed. Though it is difficult to state with certainty in the absence of more detailed x-wire measurements, it would appear that this spanwise stirring of the turbulent boundary layer profile is entirely consistent with a scenario in which the converging / diverging riblet pattern has superimposed a large-scale counter-rotating vortex array onto the boundary layer. Such a scenario would suggest that the converging portion of the riblet surface (where the flow 'converges' together) will result in a vertical flow of fluid away from the wall (forming the common-flow-up region of the counter-rotating vortex pair), while the diverging region will lead to a local mean vertical velocity component towards the wall, which will form the common-flow-down portion of the counter rotating vortex array. The common-flow-down will tend to confine the turbulent fluctuations closer to the surface (and hence lead to reduced turbulent intensity across the majority of the layer), while common-flow-up regions will move the turbulent fluctuations further from the wall, leading to increased turbulent intensity. In vortex generator studies, elevated turbulent intensities have been reported in common-flow-up regions of the vortex induced flowfield (see for example Mehta & Bradshaw, 1988). The present results are consistent with this scenario.

Experiment E2: influence of fetch F_x

Figure 4 demonstrates the effect of reduced streamwise fetch F_x. In Experiment E2 the same surface pattern as E1 is investigated at the same x location downstream of the trip and at the same freestream conditions. For E2, the only difference from E1 is that F_x has been reduced from 2.9m (approximately $60\delta_c$ or 100 000 wall units) to 1m. A comparison between figures 4 and 3 illustrates the dependance of the secondary flows on streamwise fetch. The wall-normal extent of the spanwise variation of mean velocity and turbulent intensity is much smaller for the lower value of F_x. The induced spanwise variations are confined closer to the surface for the shorter fetch, and hence the effect on the outer part of the layer is much less pronounced, with substantially less variation in boundary layer thickness. It is, however, interesting to observe from figure 4(a), that the overall strength of the spanwise variation in mean streamwise velocity U (as a percentage of the spanwise average value) remains approximately the same regardless of fetch. The results seem to indicate that the primary effect of fetch is in determining the wall-normal growth or extent of the secondary flows. The strength of the secondary flows, on the other hand, appears to be more closely associated with the convergence / divergence angle α and the viscous-scaled riblet height h^+ (see results below).

Experiment E3: influence of conv / div angle α

Figure 5 (c) and (d) show results from experiment E3, a surface with a reduced convergent / divergent angle $\alpha = 10°$. This experiment is not directly comparable with experiment E1, since it was conducted slightly further downstream from the tripped inlet to the working section (and hence the fetch F_x is also longer). However, E1 and E3 have the same freestream velocity, and hence similar viscous scaled riblet heights. It is immediately clear from comparison of E1 and E3 (comparison of figures 3 and 5 c and d), that reducing α reduces the strength of the spanwise variations induced by the surfaces. With the reduced $\alpha = 10°$, the magnitude of the spanwise variation of U at $z/\delta \approx 0.1$ is $\approx \pm 8\%$ which is much less than

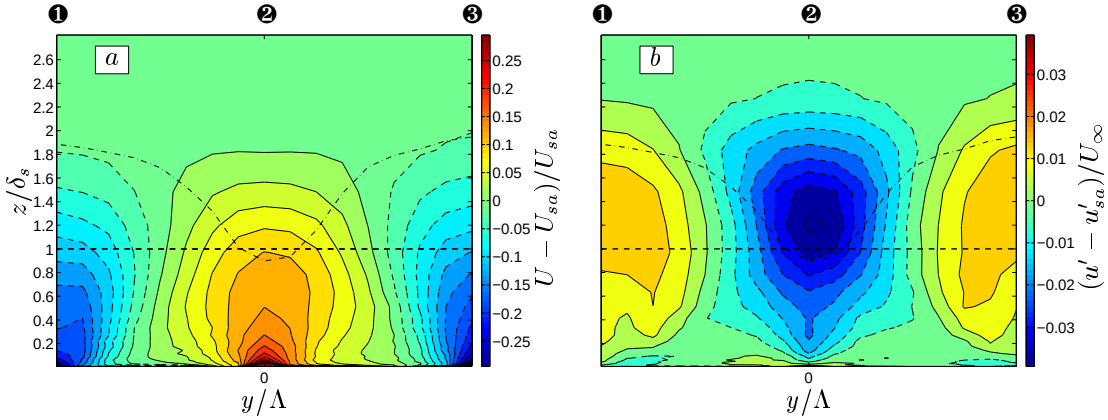

Figure 3: Spanwise variation for E1 of (a) mean velocity and (b) turbulence root-mean-squared fluctuations (u') about the spanwise averaged value for the rough wall.

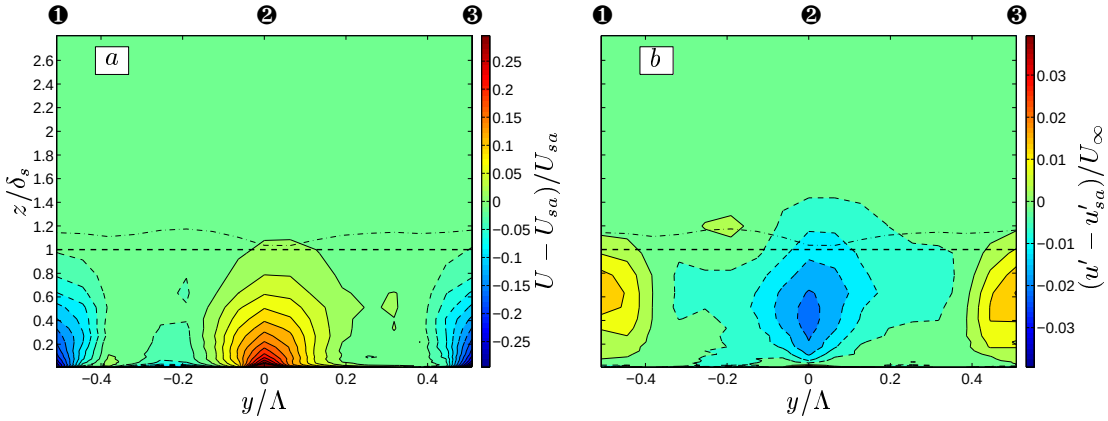

Figure 4: Spanwise variation for E2 of (a) mean velocity and (b) turbulence root-mean-squared fluctuations (u') about the spanwise averaged value for the rough wall.

the $\approx \pm 22\%$ observed for the $\alpha = 30^\circ$ case. In addition, it can be observed that the spanwise variations for E3 are confined closer to the surface, with a much less pronounced variation in δ than observed for E1 (with $\alpha = 30^\circ$ at comparable fetch).

Experiment E3 - E6: influence of h^+

Experiments E3 - E6 investigate the same surfaces but with varying freestream velocity U_∞. In this way the viscous scaled riblet height h^+ is systematically varied from $h^+ = 25$ for experiment E4, to $h^+ \approx 6$ for experiment E6 (close to the limit for hydrodynamic smoothness). From top to bottom, Figure 5 depicts this varying h^+, from $h^+ = 25$ at the top (plots a and b) to $h^+ = 6$ at the bottom (plots g and h). It should be noted that experiments E3 - E6 are not at the same Reynolds number (the friction Reynolds number reduces from approximately $Re_\tau = \delta U_\tau/\nu \approx 2500$ for E4, to $Re_\tau \approx 920$ for experiment E6). Nonetheless, it is obvious that varying the viscous-scaled riblet height has a pronounced effect on the overall strength of the three-dimensionality imposed by the surface. For the smallest viscous-scaled riblet height, figure 5(g) indicates that only very moderate percentage spanwise variations in U are observed. Clearly when the height of the riblets approach hydrodynamic smoothness, these surfaces no-longer seem capable of generating large-scale three-dimensionality.

Skin friction

At the present time these experiments lack an independent measure of the wall-shear stress τ_w. Therefore the skin friction must be estimated from the measured velocity profiles in the roughness-modified turbulent boundary layers. Standard practise for rough walls is to use a Clauser technique fitting the rough-wall data to a modified log-law region defined as,

$$U^+ = \frac{1}{\kappa} \log \hat{z}^+ + A - \Delta U^+ \qquad (1)$$

where $\hat{z}$ is defined as the wall-normal distance from the crest of the riblets plus the roughness offset ($\hat{z} = z + e$) and ΔU^+ is the roughness function (a positive number for the majority of rough surfaces, but a negative number for drag reducing surfaces such as standard riblets). The intercept of the log law, and hence the roughness function ΔU^+ can be eliminated from this fit, by differentiating equation (1) with respect to $\hat{z}^+$ to yield,

$$U_\tau = \kappa \hat{z} \frac{dU}{dz} \qquad (2)$$

The problem here being that there is one equation with

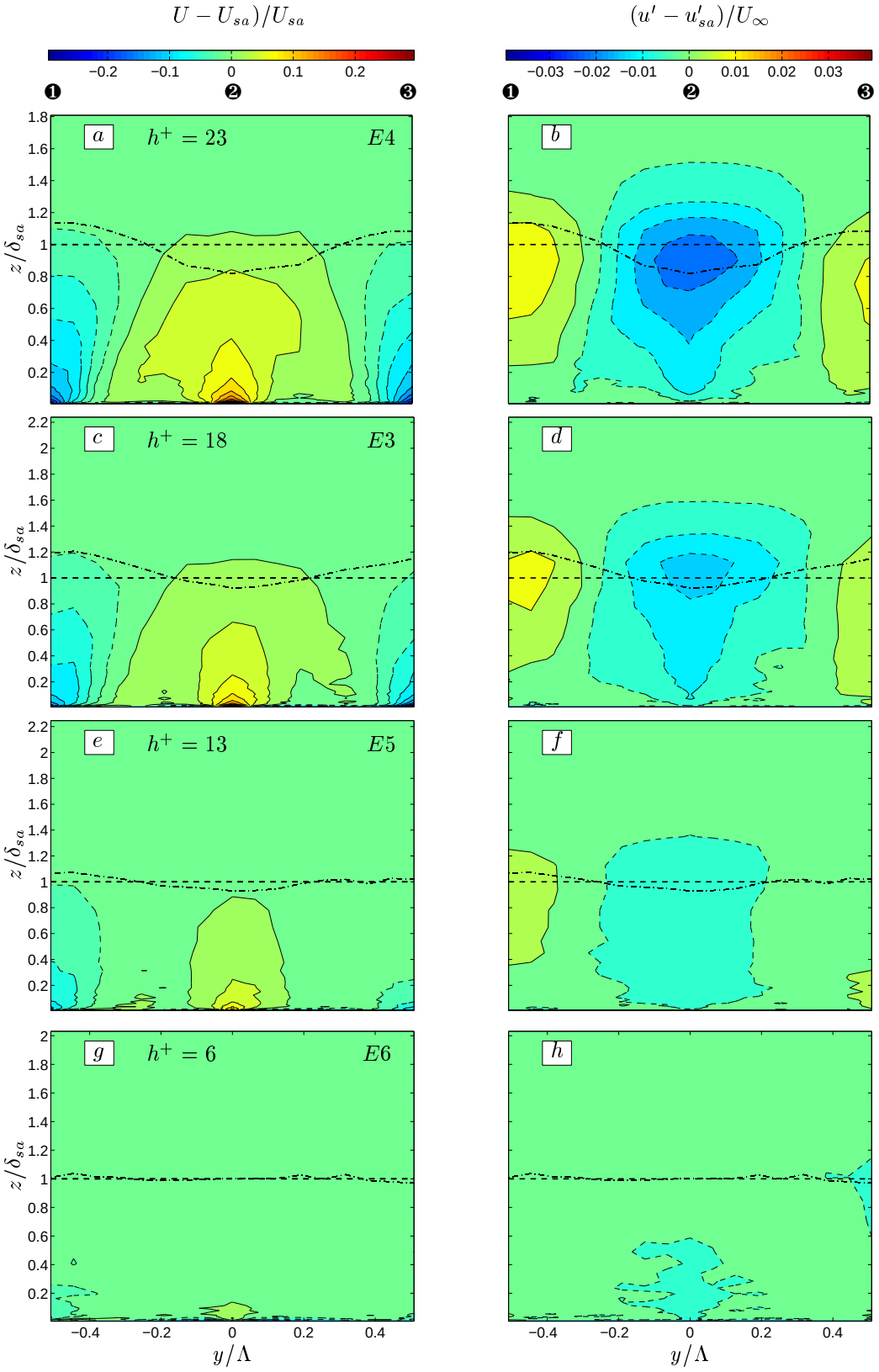

Figure 5: Spanwise variation for (right-hand-side) mean velocity and (left-hand-side) turbulence root-mean-squared fluctuations (u') about the spanwise averaged value for the rough wall experiments E3 - E6. (a & b) Experiment E4, $h^+ = 25$; (c & d) Experiment E3, $h^+ = 18$; (e & f) Experiment E5, $h^+ = 13$; (g & h) Experiment E6, $h^+ = 6$. Wall-normal position is normalised by δ_{sa} (the spanwise averaged boundary layer thickness). Dot-dashed line shows δ_{98} for rough surface. Dashed line shows spanwise averaged boundary layer thickness δ_{sa}.

two unknowns (U_τ and e), and hence the estimated value for U_τ is entirely dependant on the assumed roughness offset e. This issue becomes less important for surfaces where h/δ is a very small number (i.e higher Reynolds number riblet experiments). The error in U_τ due to an improperly determined roughness offset e is approximately 6% for $h/\delta = 1/100$, reducing to approximately 1% for $h/\delta = 1/600$. For lower Reynolds numbers it is common to assume Townsend's outer layer similarity hypothesis, and select the U_τ and e combination to best collapse the velocity defect plot in the outer and overlap regions of the flow (plotting $U_\infty - U/U_\tau$ *vs.* $\hat{z}/\delta$). It is not immediately obvious that any of these techniques will be applicable for these particular roughness surfaces where a high degree of three-dimensionality has been introduced into the flow. Indeed, the velocity profiles seem to indicate that for the converging/ diverging roughness surfaces, Townsend's outer layer similarity is not well observed (at least for the surfaces generating strong secondary flows). Figure 6 shows an attempt to determine U_τ for the surface by collapsing the mean spanwise velocity profile onto the modified law of the wall. It is evident from Figure 6(a) that the wake strength (the distance labeled $2\Pi/\kappa$) is different for the smooth and rough wall (and different for the rough wall dependent on whether over a diverging or converging region). When plotted as a velocity defect in figure 6 (b), this difference in wake strength causes a very pronounced breaking of Townsend's outer layer similarity hypothesis.

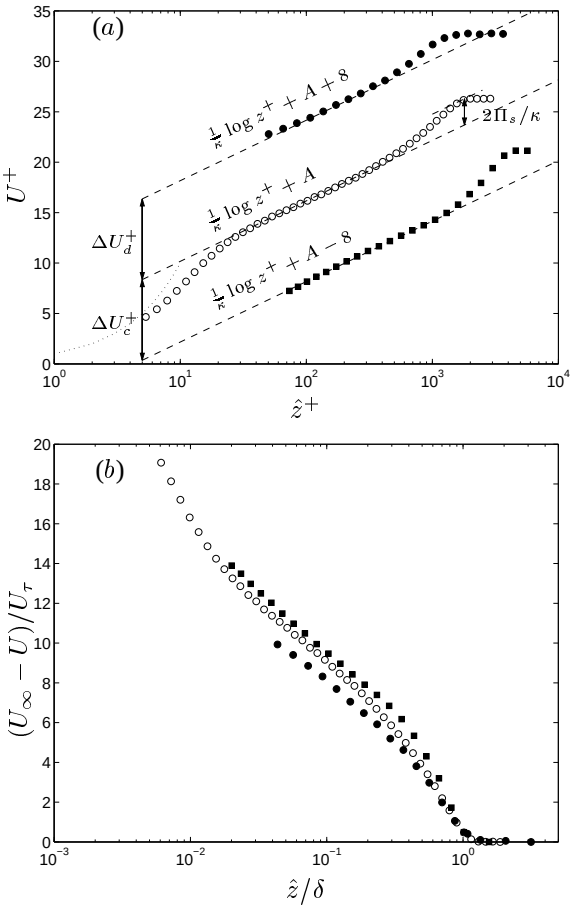

Figure 6: (a) Modified Clauser chart and (b) velocity defect plot above (○) smooth wall and rough walls; (●) diverging region (■) converging region.

4 Summary

It is shown that converging / diverging herringbone type arrangements of riblet-like striations impose large-scale secondary flows onto the turbulent boundary layer. These secondary flows lead to large-scale spanwise modifications to the mean velocity, turbulent intensity and boundary layer thickness δ. The strength and form of these secondary flows are shown to be dependant on the convergence / divergence angle α, the streamwise fetch F_x and the viscous scaled riblet height h^+. Smaller angles α lead to weaker secondary flows, and weaker spanwise variations. Increasing streamwise fetch, seems to cause enhanced wall-normal growth of the secondary flows, such that they eventually exceed the thickness of the unmodified boundary layer. There is presumably some limit to this effect, but we have not yet determined this. Increasing the viscous-scaled riblet height leads to stronger secondary flows. When h^+ approaches assumed hydrodynamic smoothness, it is seen that the strength of the secondary flows dramatically reduces. The influence of spanwise wavelength Λ has yet to be investigated, but is also presumably a key parameter.

Acknowledgments

This research was supported under the Australian Research Council's Discovery Projects funding scheme (project number DP110102448). NH is the recipient of an Australian Research Council Future Fellowship (project number FF110100432).

References

BECHERT, D., BRUSE, M., HAGE, W., VAN DER HOEVEN, J. G. & HOPPE, G. 1997 Experiments on drag-reducing surfaces and their optimisation with an adjustable geometry. *J. Fluid Mech.* **338**, 59–87.

HUTCHINS, N., NICKELS, T. B., MARUSIC, I. & CHONG, M. S. 2009 Hot-wire spatial resolution issues in wall-bounded turbulence. *J. Fluid Mech.* **635**, 103–136.

KOELTZSCH, K., DINKELACKER, A. & GRUNDMANN, R. 2002 Flow over convergent and divergent wall riblets. *Exp. Fluids* **33**, 346–350.

LIGRANI, P. M. & BRADSHAW, P. 1987 Spatial resolution and measurement of turbulence in the viscous sublayer using subminiature hot-wire probes. *Exp. Fluids* **5**, 407–417.

MEHTA, R. D. & BRADSHAW, P. 1988 Longitudinal vortices imbedded in turbulent boundary layers part2. vortex pair with 'common flow' upwards. *J. Fluid Mech.* **188**, 529–

546.